HIGH POWER LASER
SCIENCE AND ENGINEERING

RESEARCH ARTICLE

Feasibility study of laser-driven neutron sources for pharmaceutical applications

Takato Mori[1], Akifumi Yogo[1], Yasunobu Arikawa[1], Takehito Hayakawa[1,2], Seyed R. Mirfayzi[3],
Zechen Lan[1], Tianyun Wei[1], Yuki Abe[1,4], Mitsuo Nakai[1], Kunioki Mima[1], Hiroaki Nishimura[5],
Shinsuke Fujioka[1], and Ryosuke Kodama[1]

[1] *Institute of Laser Engineering, Osaka University, Suita, Japan*

[2] *National Institutes for Quantum Science and Technology, Tokai, Japan*

[3] *Tokamak Energy Ltd., Abingdon, UK*

[4] *Graduate School of Engineering, Osaka University, Suita, Japan*

[5] *Fukui University of Technology, Fukui, Japan*

Abstract
We predict the production yield of a medical radioisotope ^{67}Cu using ^{67}Zn(n, p)^{67}Cu and ^{68}Zn(n, pn)^{67}Cu reactions
with fast neutrons provided from laser-driven neutron sources. The neutrons were generated by the p+^{9}Be and d+^{9}Be
reactions with high-energy ions accelerated by laser–plasma interaction. We evaluated the yield to be $(3.3 \pm 0.5) \times 10^5$
atoms for ^{67}Cu, corresponding to a radioactivity of 1.0 ± 0.2 Bq, for a Zn foil sample with a single laser shot. Using
a simulation with this result, we estimated ^{67}Cu production with a high-frequency laser. The result suggests that it is
possible to generate ^{67}Cu with a radioactivity of 270 MBq using a future laser system with a frequency of 10 Hz and
10,000-s radiation in a hospital.

Keywords: laser ion acceleration; laser-driven neutron source; medical radioisotope

1. Introduction

Particle acceleration using lasers[1] has been studied for about four decades and, after the development of chirped pulse amplification[2], laser intensity has increased up to 10^{23} W/cm^2[3,4]. At present various particles of photons, electrons, ions and neutrons are generated by laser facilities. Ions have been accelerated by the electrostatic field generated by the electron pressure gradient, so-called target normal sheath acceleration (TNSA)[5–8]. Neutrons are generated by photodisintegration reactions with γ-rays generated by laser–plasma interactions[9], laser fusion reactions such as d(p, np)p and d(d, n)^{3}He reactions[10] or nuclear reactions by placing a secondary target behind the first target for ion acceleration[11–14]. The energies of ions accelerated by laser reach several tens of MeV, thus making it possible to generate neutrons through nuclear reactions, such as ^{7}Li(p, n)^{7}Be[11], ^{9}Be(d, xn) and ^{9}Be(p, n)[12–14]. The flux of the laser-driven neutron sources (LDNSs) has been increased up to approximately 10^{11} neutrons/sr[12–14]. Although neutrons in the MeV energy region are primarily produced by LDNSs, low-energy neutrons in thermal and epi-thermal regions can also be generated using moderators[11,15]. LDNSs have the characteristics of high brightness and short pulses, and are expected to be useful for various applications. Several experiments have demonstrated imaging using fast neutrons provided from an LDNS[16–19]. LDNSs are also expected to be used for single-shot radiography to non-destructive inspections with the combination of thermal neutrons and X-rays[20,21]. Furthermore, elemental analysis using nuclear resonance absorption with low-energy neutrons from an LDNS has been demonstrated[20].

One of the expected applications using LDNSs is the production of medical radioisotopes by a compact laser system inside of hospitals. Radioisotopes, which may radiate a γ-ray with an energy of a few hundred keV, such as ^{99m}Tc (half-life 6.02 h), are used for single-photon emission computed tomography (SPECT) in medical diagnostic scans. At present, most medical radioisotopes have been provided from nuclear reactors and accelerators, and they have been distributed to hospitals. A positron emitter ^{18}F with a

Correspondence to: Akifumi Yogo, Institute of Laser Engineering, Osaka University, Suita 565-0871, Japan. Email: yogo-a@ile.osaka-u.ac.jp

half-life of 1.8 h, which is used for positron emission tomography (PET), is produced by compact cyclotron accelerators located inside of hospitals. In addition to medical diagnostic scans, radioisotopes with half-lives of several days have been used for cancer therapy. The radioisotope ^{67}Cu with a half-life of 2.58 d is a good candidate for a radiopharmaceutical for cancer therapy because of its appropriate nuclear and chemical properties[22–24]. ^{67}Cu decays to an excited state or the ground state of the daughter nucleus ^{67}Zn through the emission of a β-ray with a maximum energy of 392, 484 or 577 keV. When an excited state is generated, it subsequently decays to the ground state of ^{67}Zn with emission of γ-rays with energies of 91, 93 and 185 keV. During therapy, a radiopharmaceutical including ^{67}Cu is accumulated inside of a tumor in a human body, therefore making the β-rays radiated from ^{67}Cu appropriate to effectively kill the cancer cells with a lethal dose. In addition, the γ-rays radiated from the ^{67}Cu-radiopharmaceutical accumulated in the cancer are suitable for SPECT imaging. Therefore, ^{67}Cu is expected to be used for radioimmunotheranostics[25], and various production methods of ^{67}Cu have been studied for future operation. ^{67}Cu production with protons and deuterons using accelerators has been studied, where ^{67}Cu is produced via ^{68}Zn(p, 2p)^{67}Cu[26,27], ^{70}Zn(p, α)^{67}Cu[23] and ^{70}Zn(d, αn)^{67}Cu reactions[28]. One of the feasible production methods is photodisintegration reactions; ^{67}Cu can be produced by the ^{68}Zn(γ, p)^{67}Cu reaction[29–31] with γ-rays provided from electron accelerators. Production by neutron-induced reactions was also studied (Figure 1). ^{67}Cu can be produced by the ^{67}Zn(n, p)^{67}Cu[32–35] and ^{68}Zn(n, np)^{67}Cu[34–36] reactions.

LDNSs provide primary fast neutrons in the energy range of 1−20 MeV, making them suitable for production of ^{67}Cu via neutron-induced reactions, as presented here. In the present study, we explore the possibility of ^{67}Cu production by LDNSs with a high-power laser. The activation method is one of the tools used to evaluate precisely the number of

unstable isotopes. In our previous studies, the numbers of fast neutrons with energies of 8−20 MeV and thermal neutrons were quantitatively evaluated using activation methods[14,37]. Here, we demonstrated ^{67}Cu production with an irradiation of laser-driven neutrons on a natural Zn metal target and measured the radioactivities of the unstable isotopes and isomer generated in the Zn target. The evaluation of the produced radioisotopes was carried out by γ-ray measurement with a high-purity germanium (HPGe) detector and we reveal the activities of ^{67}Cu and the unstable isotopes of Zn, Cu and Ni.

2. Experimental methods

The neutron irradiation experiment was carried out using the petawatt laser for fast ignition experiments (LFEX) laser system at the Institute of Laser Engineering (ILE) at Osaka University[38]. To generate and accelerate ions we focused four laser pulses provided from LFEX on a target with an intensity of approximately 1.5×10^{19} W/cm^2 and with a duration of 1.5 ps in full width at half maximum (FWHM). Figure 2 shows the experimental setup of the target installed in the vacuum chamber. The angle between the laser axis and the normal vector of the target foil was 42°. As the target, a deuterated carbon $[(C_8D_8)_n$, henceforth referred to as CD] foil with a thickness of 5 μm was used. A plasma was induced by the laser and, subsequently, ions of protons and deuterons were accelerated from the plasma via TNSA[39–41]. In the TNSA, a target foil is irradiated by a laser with an intensity higher than or equal to 10^{18} W/cm^2 to make a plasma. The generated plasma is extended into a vacuum for the opposite side (rear side) to the laser irradiation side to generate a charge separation field, by which ions on the rear surface of the target could be accelerated up to several tens of MeV. The accelerated protons and deuterons have continuous energies, of which the spectral density
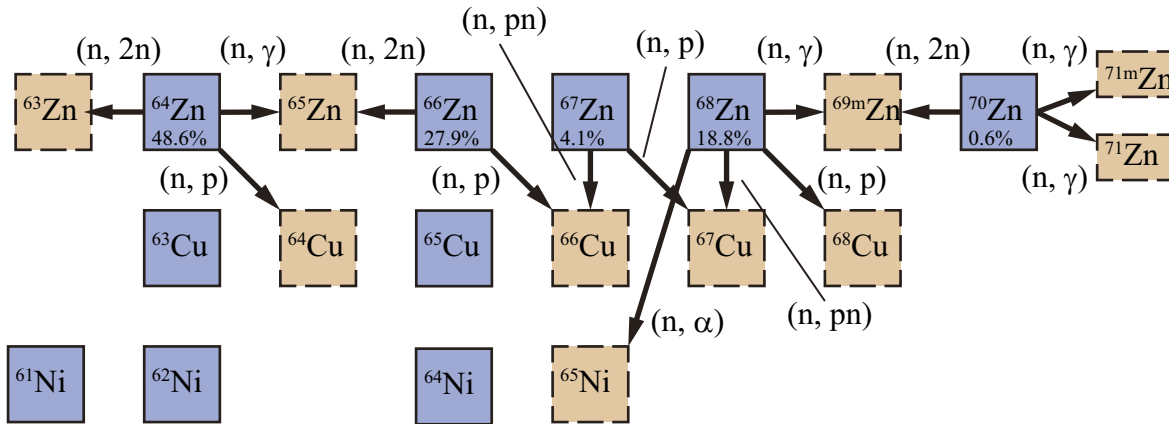

Figure 1. Partial nuclear chart around Zn and nuclear reactions with neutrons on a natural Zn target. ^{64}Cu, ^{66}Cu and ^{68}Cu are produced by (n, p) reactions with high-energy neutrons on ^{64}Zn, ^{66}Zn and ^{68}Zn, respectively. ^{63}Cu, ^{65}Cu and ^{69}Cu^m are produced by (n, 2n) reactions on ^{64}Zn, ^{66}Zn and ^{70}Zn, respectively. ^{66}Cu and ^{67}Cu^m are generated by (n, pn) reactions from ^{67}Zn and ^{86}Zn, respectively. High-energy neutrons could produce ^{65}Ni by the ^{68}Zn(n, α)^{65}Ni reaction. Neutron capture also occurs.
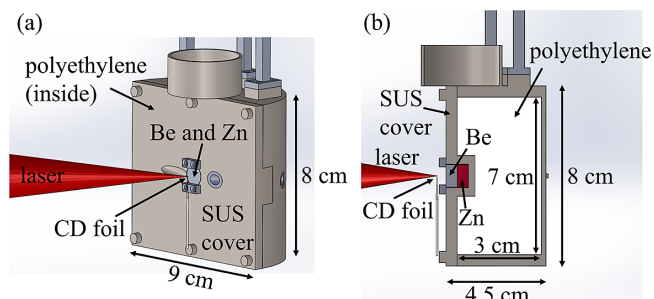
Figure 2. Experimental setup for the laser shot to generate neutrons. The laser is focused on the CD foil target. The Be neutron converter is placed 4 mm downstream of the CD foil. Behind the Be target, the Zn target was set in the hole at the center of the front surface.

decreases with increasing energies. The maximum energies of the protons and deuterons using LFEX are typically 30 and 20 MeV, respectively[42]. A Be block with a size of $\phi 10$ mm $\times 5$ mm was installed 4 mm downstream from the CD foil. The accelerated ions generated neutrons by p+^{9}Be and d+^{9}Be reactions[12–14]. High-energy neutrons are predominantly generated by the ^{9}Be(p, n)^{9}B reaction with high-energy protons. Around the Be block, a semi-cylindrical polyethylene moderator with a volume of 157 cm^3 in a stainless-steel case was located. The thicknesses of the top and side were 5 mm and the thickness of the bottom was 2 mm (see Figure 2). To produce ^{67}Cu, a natural Zn target with a size of $\phi 10$ mm $\times 5$ mm and a weight of 2.86 g was placed behind the Be target. The neutron energy spectrum was measured by the time of flight (TOF) method. A benzophenon-doped BBQ liquid scintillation detector with a size of $\phi 60$ mm $\times 60$ mm with a photomultiplier tube (PMT; Thron EMI, 9902KBT)[43] was located 8.3 m downstream from the center of the target chamber, and the angle between the laser axis and the TOF beam line was approximately 15°, corresponding to 57° away from the normal vector of the Be target. The output signal from the PMT was recorded by an oscilloscope shot by shot and the neutron energy spectrum for each laser shot was obtained from each signal[44].

Unstable isotopes and isomers were produced via nuclear reactions of the neutrons and stable isotopes of Zn. Eleven minutes after the laser shot, the Zn target was moved from the target chamber to obtain the γ-ray signals. The γ-rays emitted from the produced nuclides were measured with an HPGe detector. The efficiency of the HPGe detector relative to a $\phi 3$ inch $\times 3$ inch NaI(Tl) scintillation detector was approximately 70%. A multichannel analyzer (TechnoAP, APG7400A) was used to acquire the pulse height of the amplifier, and the dead time was less than 0.07%. Copper plates with a thickness of 5 mm and lead blocks with a thickness of 10 cm were used for background radiation shielding. Standard γ-ray sources of ^{152}Eu and ^{133}Ba were used for calibration of the detection efficiency and energy of the HPGe detector. The γ-ray measurements of the laser-neutron irradiated Zn sample and background with a

non-irradiated Zn target were conducted for 120 and 99 h, respectively, with the same background shield.

3. Experimental results

Figure 3 shows the energy spectrum of the generated neutrons, which was measured using the TOF method with the scintillation detector located 57° from the normal vector of the Be block. The maximum energy is approximately 17 MeV, and the number of neutrons decreases with increasing energy. The neutron yield was 8×10^9 neutrons/sr in the energy range from 1 MeV to the maximum energy. The maximum energy is high enough to induce the ^{67}Zn(n, p)^{67}Cu and ^{68}Zn(n, np)^{67}Cu reactions. Note that the total number and the maximum energy are expected to be lower than those of the neutrons emitted forward, respectively.

The produced radioisotopes and isomers were identified using the analysis of γ-rays radiated following β decay or internal decay of the isomers. For some nuclear species, the decay curves of γ-rays were also used for identification. The number of a produced nuclide was evaluated from the peak area in the energy spectrum. Figures 4(a)–4(c) show the γ-ray spectra from the neutron-irradiated Zn sample, the background and their subtraction in the three different energy ranges. In these spectra, the γ-rays of ^{63}Zn, ^{65}Zn, ^{69}Zn^m, ^{64}Cu, ^{66}Cu and ^{67}Cu are observed. Because the peaks of the 93 and 185-keV γ-rays radiated from ^{67}Cu in the energy spectrum were overlapped with the γ-rays from ^{234}Th and ^{235}U in the background, the background spectrum was subtracted from the Zn sample spectrum. Figures 4(d)–4(f) show the γ-ray spectra measured for 8.1 h, 5.1 h and 8 min, respectively. In Figures 4(d) and 4(e), γ-rays radiated from ^{71}Zn^m ($T_{1/2} = 4.0$ h) and ^{65}Ni ($T_{1/2} = 2.5$ h) are observed, respectively. In contrast, when the measuring time is as short as 8 min, the γ-ray peak of ^{68}Cu^m with a half-life of 3.8 min appears [see Figure 4(f)]. From the energy spectra and decay curves, ^{63}Zn, ^{65}Zn, ^{69}Zn^m, ^{71}Zn^m, ^{64}Cu, ^{66}Cu, ^{67}Cu, ^{68}Cu^m and ^{65}Ni were identified. Table 1 shows the properties and measured activities of the radioisotopes. Note that the only

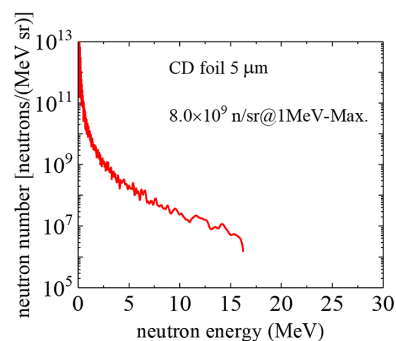**Figure 3.** Fast neutron spectrum obtained from the TOF measurement. The neutron energies reached 17 MeV.
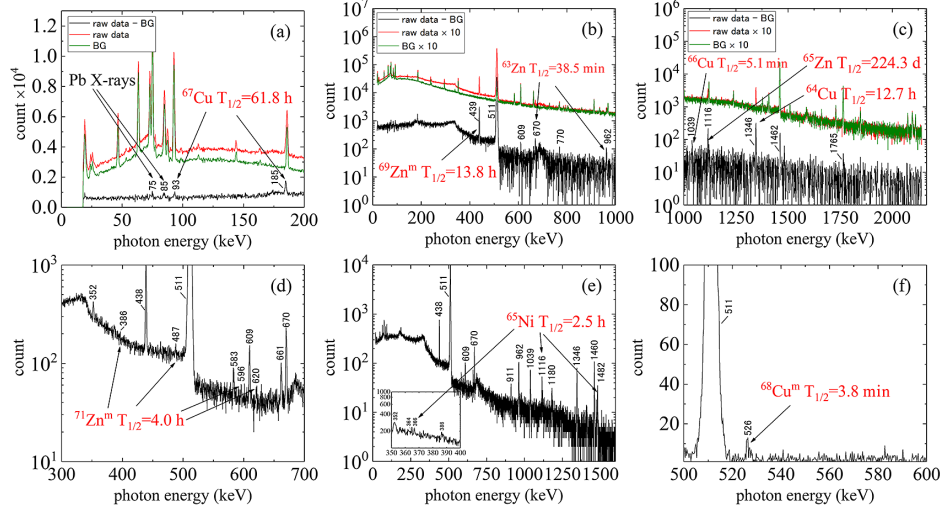
Figure 4. γ-ray spectra measured for 120 h, 8.1 h, 5.1 h and 8 min. (a)–(c) The γ-ray spectra integrated for 120 h. The background signal measured for 99 h was normalized to the target measurement of 120 h. (d) The γ-ray spectrum measured for 8.1 h, where peaks corresponding to $^{71}Zn^m$ are observed. (e) The γ-ray spectrum for 5.1 h, where peaks for ^{65}Ni are observed. (f) The γ-ray spectrum for 8 min, which shows the $^{68}Cu^m$ peak at 526 keV.

Table 1. Produced nuclides and their half-lives, γ-ray energies, emission probabilities of the γ-rays, nuclear reactions, numbers and activities.

Nuclide	$T_{1/2}$	E_γ (keV)	I_γ (%)	Nuclear reaction	Quantities of the nuclides	Activity (Bq) $t = 0$ h	$t = 12$ h
^{63}Zn	38.47 min	669.62	8	$^{64}Zn(n, 2n)$	$(9.3 \pm 0.8) \times 10^5$	$(28 \pm 2) \times 10$	$(6.5 \pm 0.6) \times 10^{-4}$
		962.06	6.5				
^{65}Zn	224.26 d	1115.55	50.6	$^{64}Zn(n, \gamma)$ and $^{66}Zn(n, 2n)$	$(1.45 \pm 0.15) \times 10^7$	0.52 ± 0.05	$(5.2 \pm 0.5) \times 10^{-1}$
$^{69}Zn^m$	13.76 h	438.6	94.77	$^{68}Zn(n, \gamma)$ and $^{70}Zn(n, 2n)$	$(6.6 \pm 0.4) \times 10^5$	9.2 ± 0.6	5.0 ± 0.3
^{71}Zn	2.45 min	910.27	7.8	$^{70}Zn(n, \gamma)$	$< 1.5 \times 10^5$	< 710	$< 2.4 \times 10^{-86}$
$^{71}Zn^m$	3.96 h	386.28	93	$^{70}Zn(n, \gamma)$	$(1.9 \pm 0.5) \times 10^4$	0.8 ± 0.2	$(1.1 \pm 0.3) \times 10^{-1}$
		487.38	62				
		596.14	27.9				
		620.18	57				
^{64}Cu	12.7 h	1345.84	0.473	$^{64}Zn(n, p)$	$(5.9 \pm 0.5) \times 10^7$	$(89 \pm 8) \times 10$	$(4.7 \pm 0.4) \times 10^2$
^{66}Cu	5.12 min	1039.23	9	$^{66}Zn(n, p)$ and $^{67}Zn(n, np)$	$(2.03 \pm 0.25) \times 10^6$	$(458 \pm 56) \times 10$	$(2.1 \pm 0.3) \times 10^{-39}$
^{67}Cu	61.83 h	93.3	16.1	$^{67}Zn(n, p), {}^{68}Zn(n, np)$	$(3.3 \pm 0.5) \times 10^5$	1.0 ± 0.2	$(9.0 \pm 1.4) \times 10^{-1}$
		184.6	48.7				
$^{68}Cu^m$	3.75 min	525.9	73	$^{68}Zn(n, p)$	$(3.2 \pm 1.4) \times 10^4$	99 ± 43	$(1.6 \pm 0.7) \times 10^{-56}$
^{65}Ni	2.52 h	366.27	4.81	$^{68}Zn(n, \alpha)$	$(1.8 \pm 0.2) \times 10^5$	14 ± 2	$(5.1 \pm 0.6) \times 10^{-1}$
		1115.55	15.43				
		1481.84	24				

upper limit of the radioactivity of ^{71}Zn was obtained by taking the square root of background around 910.27 keV. Although the 511.56-keV γ-ray with a highest emission probability of 32% is radiated from ^{71}Zn, it is difficult to use it for the estimation of radioactivity because its energy is nearly equal to 511 keV, which is one of the strongest background γ-rays.

4. Discussion

In the present study, we revealed that the radioisotope ^{67}Cu was generated by nuclear reactions on the natural Zn target with laser-driven neutrons, and obtained $(3.3 \pm 0.5) \times 10^5$ atoms of ^{67}Cu corresponding to the radioactivity of 1.0 ± 0.2 Bq for ^{67}Cu using only a single laser shot. We evaluated

the expected radioactivity of ^{67}Cu and the other isotopes measured in the present experiment using the PHITS version 3.08 Monte Carlo simulation code[45]. The cross-sections of the nuclear reactions were taken from the JENDL–4.0 nuclear data library[46], as shown in Figure 5. Note that although the cross-sections at energies higher than 20 MeV are not included in the database, this upper limit is higher than the maximum energy of the neutrons assumed in the calculation. We calculated the radioactivities for the present experimental setup, and the measured neutron spectrum, as shown in Figure 4, was used as input data. The results are also presented in Table 2. There is disagreement between the experimental and calculated values. As listed in Table 2, the calculated radioactivities are lower than the measured values by a factor of 2.8−200. The measured radioactivity
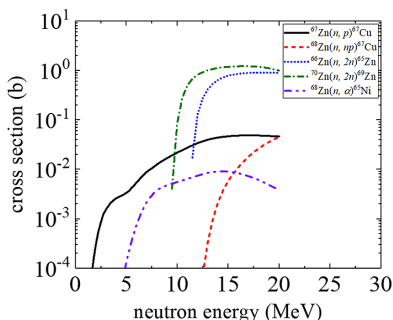
Figure 5. Cross sections used in the simulation calculation, which are taken from the JENDL-4.0 nuclear data library.

Table 2. Experimental activities, calculated activities and their ratio of the obtained activities in the present experiment. The calculated activities were obtained using the PHITS simulation code with the measured neutron energy spectrum.

Nuclide	Activity (Bq)		
	Experiment	Simulation	Exp/Sim ratio
^{63}Zn	$(282 \pm 2) \times 10$	1.40	200
^{65}Zn	0.52 ± 0.05	0.19	2.8
^{69}Zn^m	9.2 ± 0.6	1.4	6.6
^{71}Zn	<710	30.6	<23
^{71}Zn^m	0.8 ± 0.2	0.04	20
^{64}Cu	$(89 \pm 8) \times 10$	37.2	23.9
^{66}Cu	$(458 \pm 56) \times 10$	59.2	77.4
^{67}Cu	1.0 ± 0.2	0.02	50
^{68}Cu^m	99 ± 43	0.84	118
^{65}Ni	14 ± 2	0.35	40

of ^{67}Cu is 50 times larger than the calculated one. This discrepancy suggests that the number of the high-energy neutrons irradiating on the Zn target is more than the value assumed in the present calculation. This probably comes from the fact that the neutron energy spectrum used as the input was measured at $57°$. Because the neutron density is, in general, the largest at the forward angle, the assumed neutron flux and the maximum energy are considered to be lower than the actual values. Thus, we multiply the calculated yield of ^{67}Cu by the scaling factor of 50 in the following discussion.

Radioisotopic impurity is one of the key parameters for the realization of a radiopharmaceutical. To evaluate the radioisotopic impurity, we also evaluated the radioactivities of other isotopes, as listed in Table 2. The radioactivities of ^{63}Zn, ^{69}Zn^m, ^{64}Cu, ^{66}Cu, ^{68}Cu^m and ^{65}Ni are stronger than that of ^{67}Cu by one to three orders of magnitude. In general, the Zn and Ni isotopes could be separated from the Cu isotopes with chemical processes[47]. Among the Cu isotopes, because the half-lives of ^{66}Cu and ^{68}Cu^m are shorter than 6 min, after the cooling time of 12 h their activities decrease lower than 10^{-40} Bq (see Table 1). Even if we use chemical separation and cooling processes, the unstable isotope ^{64}Cu still remains. ^{64}Cu is predominantly produced by the ^{64}Zn(n, p)^{64}Cu reaction on the stable isotope ^{64}Zn

with an isotopic fraction of 48.6%. To decrease the impurity of ^{64}Cu, when we use the isotope enriched target of ^{67}Zn or ^{68}Zn, in which the isotopic fraction of ^{64}Zn is lower than 0.0486%, it is possible to decrease the ^{64}Cu radioactivity lower than 0.47 Bq. The experiment/simulation ratio for ^{64}Cu is 23.9, as listed in Table 2, which is lower than that for ^{67}Cu. This is because ^{67}Cu is produced by the ^{68}Zn(n, np)^{67}Cu reaction with relatively high-energy neutrons, but ^{64}Cu cannot be produced by the ^{65}Zn(n, np)^{64}Cu reaction on the unstable isotope ^{65}Zn. Thus, when we use relatively high-energy neutrons, the radioactivity of ^{64}Cu decreases.

To estimate the activity of ^{67}Cu that can be produced in hospitals, we calculate a possible yield of ^{67}Cu using a laser for an optimized target system, as shown in Figure 6. We assume an enriched ^{67}Zn target for neutron irradiation. A well-type Zn target has a $\phi30$ cm$\times3$ cm size with a hole of $\phi5$ cm$\times15$ cm. The volume of the Zn target is approximately 2.1×10^4 cm^3. In the bottom of the hole, the Be neutron generation target is located. The unstable isotope ^{67}Cu is predominantly produced via the ^{67}Zn(n, p)^{67}Cu reaction with neutrons with energies up to 17 MeV. We finally obtain the expected radioactivity of approximately 54 Bq for a single laser shot without the scaling factor of 50. Although we used a low-frequency high-power laser for the present demonstration, a high-frequency laser will be most efficient for the laser system placed inside hospitals because of its compactness and ability to provide laser intensity higher than 10^{20} W/cm^2, leading to effective neutron generation. If we irradiate the laser-driven neutrons in the condition as assumed above for 10,000 s with a frequency of 10 Hz, we can obtain approximately 270 MBq of ^{67}Cu with the scaling factor. This result suggests the possibility of production of medical radioisotopes using LDNSs in hospitals, although further studies are required for more realistic estimation.

5. Summary

In this study, we have demonstrated production of a medical radioisotope, ^{67}Cu, using LFEX at Osaka University. Neutrons with energies of up to 17 MeV have been generated using p+^{9}Be and d+^{9}Be reactions on the secondary target located behind the ion acceleration target. The neutron energy spectrum at $57°$ is obtained from the TOF method. The radioactivities of the generated unstable isotopes and isomers were evaluated from γ-ray energy spectra measured with an HPGe detector. The ^{67}Cu radioactivity of 1.0 ± 0.2 Bq was obtained, which is about 50 times higher than the value calculated using the PHITS simulation code. This may originate from the fact that the neutron energy spectrum was measured at $57°$ and, thus, the maximum energy and total number are lower than those of the neutrons irradiating on the Zn target. We estimated radioactivity of ^{67}Cu using a future laser system and the PHITS code, obtaining the result that it is possible to produce 270 MBq
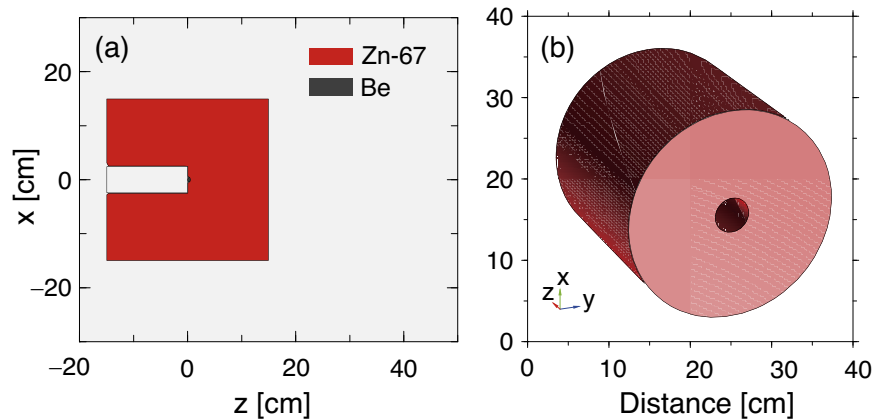
Figure 6. Geometry of the calculation of the yield of ^{67}Cu using a laser for an optimized target system. (a) Cross-sectional view of the Be and ^{67}Zn target. (b) 3D image of the target.

of ^{67}Cu using a high-frequency laser for 10,000 s irradiation. This suggests that the medical radioisotope may be produced in a compact laser system inside of a hospital in the future.

References

1. T. Tajima and J. M. Dawson, Phys. Rev. Lett. **43**, 267 (1979).
2. D. Strickland and G. Mourou, Opt. Commun. **56**, 219 (1985).
3. G. A. Mourou, T. Tajima, and S. V. Bulanov, Rev. Mod. Phys. **78**, 309 (2006).
4. K. A. Tanaka, K. M. Spohr, D. L. Balabanski, S. Balascuta, L. Capponi, M. O. Cernaianu, M. Cuciuc, A. Cucoanes, I. Dancus, A. Dhal, B. Diaconescu, D. Doria, P. Ghenuche, D. G. Ghita, S. Kisyov, V. Nastasa, J. F. Ong, F. Rotaru, D. Sangwan, P.-A. Söderström, D. Stutman, G. Suliman, O. Tesileanu, L. Tudor, N. Tsoneva, C. A. Ur, D. Ursescu, and N. V. Zamfir, Matter Radiat. Extrememes **5**, 024402 (2020).
5. R. A. Snavely, M. H. Key, S. P. Hatchett, T. E. Cowan, M. Roth, T. W. Phillips, M. A. Stoyer, E. A. Henry, T. C. Sangster, M. S. Singh, S. C. Wilks, A. MacKinnon, A. Offenberger, D. M. Pennington, K. Yasuike, A. B. Langdon, B. F. Lasinski, J. Johnson, M. D. Perry, and E. M. Campbell, Phys. Rev. Lett. **85**, 2945 (2000).
6. A. G. S. Maksimchuk, K. Flippo, D. Umstadter, and V. Y. Bychenkov, Phys. Rev. Lett. **84**, 4108 (2000).
7. S. P. Hatchett, C. G. Brown, T. E. Cowan, E. A. Henry, J. S. Johnson, M. H. Key, J. A. Koch, A. B. Langdon, B. F. Lasinski, R. W. Lee, A. J. Mackinnon, D. M. Pennington, M. D. Perry, T. W. Phillips, M. Roth, T. C. Sangster, M. S. Singh, R. A. Snavely, M. A. Stoyer, S. C. Wilks, and K. Yasuike, Phys. Plasmas **7**, 2076 (2000).
8. S. C. Wilks, A. B. Langdon, T. E. Cowan, M. Roth, M. Singh, S. Hatchett, M. H. Key, D. Pennington, A. MacKinnon, and R. A. Snavely, Phys. Plasmas **8**, 542 (2001).
9. Y. Arikawa, M. Utsugi, M. Alessio, T. Nagai, Y. Abe, S. Kojima, S. Sakata, H. Inoue, S. Fujioka, Z. Zhang, H. Chen, J. Park, J. Williams, T. Morita, Y. Sakawa, Y. Nakata,

J. Kawanaka, T. Jitsuno, N. Sarukura, N. Miyanaga, M. Nakai, H. Shiraga, H. Nishimura, and H. Azechi, Plasma Fusion Res. **10**, 2404003 (2015).
10. S. Kar, A. Green, H. Ahmed, A. Alejo, A. P. L. Robinson, M. Cerchez, R. Clarke, D. Doria, S. Dorkings, J. Fernandez, S. R. Mirfayzi, P. McKenna, K. Naughton, D. Neely, P. Norreys, C. Peth, H. Powell, J. A. Ruiz, J. Swain, O. Willi, and M. Borghesi, New J. Phys. **18**, 053002 (2016).
11. S. R. Mirfayzi, A. Alejo, H. Ahmed, D. Raspino, S. Ansell, L. A. Wilson, C. Armstrong, N. M. H. Butler, R. J. Clarke, A. Higginson, J. Kelleher, C. D. Murphy, M. Notley, D. R. Rusby, E. Schooneveld, M. Borghesi, P. McKenna, N. J. Rhodes, D. Neely, C. M. Brenner, and S. Kar, Appl. Phys. Lett. **111**, 044101 (2017).
12. A. Kleinschmid, V. Bagnoud, O. Deppert, A. Favalli, S. Frydrych, J. Hornung, D. Jahn, G. Schaumann, A. Tebartz, F. Wagner, G. Wurden, B. Zielbauer, and M. Roth, Phys. Plasmas **25**, 053101 (2018).
13. A. Favalli, N. Guler, D. Henzlova, S. Croft, K. Falk, D. C. Gautier, K. D. Ianakiev, M. Iliev, S. Palaniyappan, M. Roth, J. C. Fernandez, and M. T. Swinhoe, Sci. Rep. **9**, 2004 (2019).
14. T. Mori, A. Yogo, T. Hayakawa, S. R. Mirfayzi, Z. Lan, Y. Abe, Y. Arikawa, D. Golovin, T. Wei, Y. Honoki, M. Nakai, K. Mima, H. Nishimura, S. Fujioka, and R. Kodama, Phys. Rev. C **104**, 015808 (2021).
15. S. R. Mirfayzi, A. Yogo, Z. Lan, T. Ishimoto, A. Iwamoto, M. Nagata, M. Nakai, Y. Arikawa, Y. Abe, D. Golovin, Y. Honoki, T. Mori, K. Okamoto, S. Shokita, D. Neely, S. Fujioka, K. Mima, H. Nishimura, S. Kar, and R. Kodama, Sci. Rep. **10**, 20157 (2020).
16. M. Roth, D. Jung, K. Falk, N. Guler, O. Deppert, M. Devlin, A. Favalli, J. Fernandez, D. Gautier, M. Geissel, R. Haight, C. E. Hamilton, B. M. Hegelich, R. P. Johnson, F. Merrill, G. Schaumann, K. Schoenberg, M. Schollmeier, T. Shimada, T. Taddeucci, J. L. Tybo, F. Wagner, S. A. Wender, C. H. Wilde, and G. A. Wurden, Phys. Rev. Lett. **110**, 044802 (2013).
17. N. Guler, P. Volegov, A. Favalli, F. E. Merrill, K. Falk, D. Jung, J. L. Tybo, C. H. Wilde, S. Croft, C. Danly, O. Deppert, M. Devlin, J. Fernandez, D. C. Gautier, M. Geissel, R. Haight, C. E. Hamilton, B. M. Hegelich, D. Henzlova, R. P. Johnson, G. Schaumann, K. Schoenberg, M. Schollmeier, T. Shimada, M. T. Swinhoe, T. Taddeucci, S. A. Wender, G. A. Wurden, and M. Roth, J. Appl. Phys. **120**, 154901 (2016).
18. R. Mizutani, Y. Abe, Y. Arikawa, J. Nishibata, A. Yogo, S. R. Mirfayzi, H. Nishimura, K. Mima, S. Fujioka, M. Nakai, H. Shiraga, and R. Kodama, High Energy Density Phys. **36**, 100833 (2020).

19. K. Mima, A. Yogo, S. R. Mirfayzi, Z. Lan, Y. Arikawa, Y. Abe, and H. Nishimura, Appl. Opt. **61**, 2398 (2022).

20. A. Yogo, S. R. Mirfayzi, Y. Arikawa, Y. Abe, T. Wei, T. Mori, Z. Lan, Y. Hoonoki, D. O. Golovin, K. Koga, Y. Suzuki, M. Kanasaki, S. Fujioka, M. Nakai, T. Hayakawa, K. Mima, H. Nishimura, S. Kar, and R. Kodama, Appl. Phys. Express **14**, 106001 (2021).

21. T. Wei, A. Yogo, T. Hayakawa, Y. Arikawa, Y. Abe, M. Nakanishi, S. R. Mirfayzi, Z. Lan, T. Mori, K. Mima, S. Fujioka, M. Murakami, M. Nakai, H. Nishimura, S. Kar, and R. Kodama, AIP Adv. **12**, 045220 (2022).

22. I. Novak-Hofer and P. A. Schubiger, Eur. J. Nucl. Med. **29**, 821 (2002).

23. S. Mirzadeh, L. F. Mausner, and S. C. Srivastava, Appl. Radiat. Isot. **37**, 29 (1986).

24. N. A. Smith, D. Bowers, and D. A. Ehst, Appl. Radiat. Isot. **70**, 2377 (2012).

25. G. Ting, C.-H. Chang, H.-E. Wang, and T.-W. Lee, J. Biomed. Biotechnol. **2010**, 953537 (2010).

26. A. K. Dasgupta, L. F. Mausner, and S. C. Srivastava, Appl. Radiat. Isot. **42**, 371 (1991).

27. T. Katabuchi, S. Watanabe, N. S. Ishioka, Y. Iida, H. Hanaoka, K. Endo, and S. Matsuhashi, J. Radioanal. Nucl. Chem. **277**, 467 (2008).

28. J. Kozempel, K. Abbas, F. Simonelli, A. Bulgheroni, U. Holzwarth, and N. Gibson, Radiochim. Acta **100**, 419 (2012).

29. M. Yagi and K. Kondo, Appl. Radiat. Isot. **29**, 757 (1978).

30. P. Polak, J. Geradts, R. Vlist, and L. Lindner, Radiochimica Acta **40**, 169 (1986).

31. G. H. Hovhannisyan, T. M. Bakhshiyan, and R. K. Dallakyanc, Nucl. Instrum. Methods Phys. Res. Sect. B **498**, 48 (2021).

32. L. F. Mausner, K. L. Kolsky, V. Joshi, and S. C. Srivastava, Appl. Radiat. Isot. **49**, 285 (1998).

33. M. Al-Abyad, I. Spahn, S. Sudar, M. Morsy, M. N. H. Comsan, J. Csikai, S. M. Qaim, and H. H. Coenen, Appl. Radiat. Isot. **64**, 717 (2006).

34. T. Kin, Y. Nagai, N. Iwamoto, F. Minato, O. Iwamoto, Y. Hatsukawa, M. Segawa, H. Harada, C. Konno, K. Ochiai, and K. Takakura, J. Phys. Soc. Jpn. **82**, 034201 (2013).

35. M. Kawabata, S. Motoishi, A. Ota, A. Motomura, H. Saeki, K. Tsukada, S. Hashimoto, N. Iwamoto, Y. Nagai, and K. Hashimoto, J. Radioanal. Nucl. Chem. **330**, 913 (2021).

36. N. Sato, K. Tsukada, S. Watanabe, N. S. Ishioka, M. Kawabata, H. Saeki, Y. Nagai, T. Kin, F. Minato, N. Iwamoto, and O. Iwamoto, J. Phys. Soc. Jpn. **83**, 073201 (2014).

37. T. Mori, A. Yogo, T. Hayakawa, S. R. Mirfayzi, Z. Lan, T. Wei, Y. Abe, Y. Arikawa, M. Nakai, K. Mima, H. Nishimura, S. Fujioka, and R. Kodama, J. Phys. G **49**, 065103 (2022).

38. J. Kawanaka, N. Miyanaga, H. Azechi, T. Kanabe, T. Jitsuno, K. Kondo, Y. Fujimoto, N. Morio, S. Matsuo, Y. Kawakami, R. Mizoguchi, K. Tauchi, M. Yano, S. Kudo, and Y. Ogura, J. Phys. Conf. Ser. **112**, 032006 (2008).

39. J. Fuchs, P. Antici, E. d'Humières, E. Lefebvre, M. Borghesi, E. Brambrink, C. A. Cecchetti, M. Kaluza, V. Malka, M. Manclossi, S. Meyroneinc, P. Mora, J. Schreiber, T. Toncian, H. Pépin, and P. Audebert, Nat. Phys. **2**, 48 (2006).

40. J. Fuchs, Y. Sentoku, E. d'Humières, T. E. Cowan, J. Cobble, P. Audebert, A. Kemp, A. Nikroo, P. Antici, E. Brambrink, A. Blazevic, E. M. Campbell, J. C. Fernández, J.-C. Gauthier, M. Geissel, M. Hegelich, S. Karsch, H. Popescu, N. Renard-LeGalloudec, M. Roth, J. Schreiber, R. Stephens, and H. Pépin, Phys. Plasmas **14**, 053105 (2007).

41. A. Yogo, K. Mima, N. Iwata, S. Tosaki, A. Morace, Y. Arikawa, S. Fujioka, T. Johzaki, Y. Sentoku, H. Nishimura, A. Sagisaka, K. Matsuo, N. Kamitsukasa, S. Kojima, H. Nagatomo, M. Nakai, H. Shiraga, M. Murakami, S. Tokita, J. Kawanaka, N. Miyanaga, K. Yamanoi, T. Norimatsu, H. Sakagami, S. V. Bulanov, K. Kondo, and H. Azechi, Sci. Rep. **7**, 42451 (2017).

42. D. O. Golovin, S. R. Mirfayzi, S. Shokita, Y. Abe, Z. Lan, Y. Arikawa, A. Morace, T. A. Pikuz, and A. Yogo, J. Instrument. **16**, T02005 (2021).

43. Y. Abe, H. Hosoda, Y. Arikawa, T. Nagai, S. Kojima, S. Sakata, H. Inoue, Y. Iwasa, K. Iwano, K. Yamanoi, S. Fujioka, M. Nakai, N. Sarukura, H. Shiraga, T. Norimatsu, and H. Azechi, Rev. Sci. Instrum. **85**, 11E126 (2014).

44. S. R. Mirfayzi, S. Kar, H. Ahmed, A. G. Krygier, A. Green, A. Alejo, R. Clarke, R. R. Freeman, J. Fuchs, D. Jung, A. Kleinschmidt, J. T. Morrison, Z. Najmudin, H. Nakamura, P. Norreys, M. Oliver, M. Roth, L. Vassura, M. Zepf, and M. Borghesi, Rev. Sci. Instrum. **86**, 073308 (2015).

45. T. Sato, Y. Iwamoto, S. Hashimoto, T. Ogawa, T. Furuta, S.-i. Abe, T. Kai, P.-E. Tsai, N. Matsuda, H. Iwase, N. Shigyo, L. Sihver, and K. Niita, J. Nucl. Sci. Technol. **55**, 684 (2018).

46. K. Shibata, O. Iwamoto, T. Nakagawa, N. Iwamoto, A. Ichihara, S. Kunieda, S. Chiba, K. Furutaka, N. Otuka, T. Ohsawa, T. Murata, H. Matsunobu, A. Zukeran, S. Kamada, and J.-I. Katakura, J. Nucl. Sci. Technol. **48**, 1 (2011).

47. S. Watanabe, Y. Iida, N. Suzui, T. Katabuchi, S. Ishii, N. Kawachi, H. Hanaoka, S. Matsuhashi, K. Endo, and N. Ishioka, J. Radioanal. Nucl. Chem. **280**, 199 (2009).